Elucidation of the Strongest Factors Influencing Rapid Retinal Nerve Fiber Layer Thinning in Glaucoma

Eun Ji Lee,[1] Tae-Woo Kim,[1] Ji-Ah Kim,[1] Gyu-Nam Kim,[1] Joon Mo Kim,[2] Michaël J. A. Girard,[3,4] Jean Martial Mari,[5] and Hyunjoong Kim[6]

[1]Department of Ophthalmology, Seoul National University College of Medicine, Seoul National University Bundang Hospital, Seongnam, Korea
[2]Department of Ophthalmology, Kangbuk Samsung Hospital, Sungkyunkwan University School of Medicine, Seoul, Korea
[3]Department of Biomedical Engineering, National University of Singapore, Singapore
[4]Singapore Eye Research Institute, Singapore National Eye Centre, Singapore
[5]GePaSud, Université de la Polynésie Française, Tahiti, French Polynesia
[6]Department of Applied Statistics, Yonsei University, Seoul, Korea

Correspondence: Tae-Woo Kim, Department of Ophthalmology, Seoul National University Bundang Hospital, Seoul National University College of Medicine 82, Gumi-ro, 173 Beongil, Bundang-gu, Seongnam, Gyeonggi-do 463–707, Korea; twkim7@snu.ac.kr.
Joon Mo Kim, Department of Ophthalmology, Kangbuk Samsung Hospital, Sungkyunkwan University School of Medicine, 29 Saemunan-ro, Jongno-gu, Seoul 03181, Korea; kjoonmo1@gmail.com.

Submitted: December 27, 2018
Accepted: July 9, 2019

Citation: Lee EJ, Kim T-W, Kim J-A, et al. Elucidation of the strongest factors influencing rapid retinal nerve fiber layer thinning in glaucoma. *Invest Ophthalmol Vis Sci*. 2019;60:3343–3351. https://doi.org/10.1167/iovs.18-26519

Purpose. To determine which groupings of prognostic factors best explain the rapid progressive retinal nerve fiber layer (RNFL) thinning in patients with primary open-angle glaucoma (POAG).

Methods. Optic nerves of 111 POAG patients who were followed for at least 2.5 years, during which the RNFL thickness was measured by serial spectral-domain optical coherence tomography (OCT) were included. Eyes were imaged using enhanced depth-imaging spectral-domain OCT and swept-source OCT angiography to determine the lamina cribrosa curvature index (LCCI), and the presence of a choroidal microvasculature dropout (cMvD), respectively. The rate of RNFL thinning was determined by linear regression of serial OCT RNFL thickness measurements. A regression tree model was used to find groupings of factors that best explain the rate of future RNFL thinning.

Results. Disc hemorrhage, larger LCCI, and presence of cMvD were associated with faster global RNFL thinning in the multivariate regression analysis. The regression tree analysis revealed three stratified groups based on the rate of RNFL thinning, divided by the LCCI and the presence of cMvD. Eyes with LCCI $\geq$11.87 had the fastest RNFL thinning (-2.4 ± 0.8 μm/year, mean $\pm$ SD). Among eyes with LCCI <11.87, the presence of cMvD was the strongest factor influencing faster RNFL thinning (-1.5 ± 0.8 μm/year). Eyes with LCCI <11.87 and without a cMvD exhibited the slowest RNFL thinning (-0.8 ± 0.9 μm/year).

Conclusions. Our regression tree model demonstrated that larger LCCI, and then the presence of cMvD were the first and second strongest prognostic factors for faster progressive RNFL thinning. Further studies may be needed to confirm these findings.

Keywords: glaucoma progression, optical coherence tomography angiography, lamina cribrosa, choroidal microvasculature

According to the mechanical theory of glaucoma, posterior deformation of the lamina cribrosa (LC) is the principal event that induces axonal damage in this condition.[1–4] The LC deformation induced by stress related to the IOP is thought to promote the death of retinal ganglion cells via various mechanisms, including blockade of axoplasmic flow and tissue remodeling by reactive astrocytes.[5–9] Consistent with this concept, recent imaging studies using optical coherence tomography (OCT) found that the degree of LC deformation as quantified by the LC depth or LC curvature was associated with the rate of progressive retinal nerve fiber layer (RNFL) thinning in eyes with glaucoma[10] and suspected glaucoma.[11]

However, a smaller degree of LC deformation does not guarantee slower disease progression. Although no studies have specifically focused on this issue, the data obtained in previous studies have shown that rapid progression still occurs despite a small LC depth or a small LC curvature in some patients. This finding indicates that the future disease outcome cannot be predicted solely based on the degree of LC deformation.

Glaucoma progression is known to be affected by various factors that are not directly related to mechanical stress.[12] Vascular factors, such as low blood pressure[13–15] and primary vascular dysregulation,[15,16] have been recognized as risk factors for glaucoma progression. In addition, ocular factors including β-zone parapapillary atrophy (PPA)[17–20] and disc hemorrhage (DH)[13,21–23] have also been consistently identified as prognostic variables. Park et al.[24] recently found localized microvasculature dropout in the parapapillary choroid as shown by OCT angiography (OCTA) to be associated with faster progressive RNFL thinning in primary open-angle glaucoma (POAG).

Given that glaucoma progression is affected by diverse factors, the disease prognosis could be better predicted when multiple factors are considered together. The purpose of this study was to develop a systematic prognostic model for the future rate of progressive RNFL thinning in POAG eyes, based

on integrating various factors that are potentially associated with glaucoma progression. This was achieved by applying a regression tree analysis (recursive partitioning tree),[25] which is an interactive statistical tool used to separate a group into two subgroups repeatedly based on certain risk factors of interest. This approach has the advantage of creating a prognostic model based on the combination of factors that can best explain different rates of progression.

Methods

Participants

This study involved POAG patients who were enrolled in the Investigating Glaucoma Progression Study, which is an ongoing prospective study of glaucoma patients at the Glaucoma Clinic of Seoul National University Bundang Hospital. All subjects provided written informed consent to participate. The study protocol was approved by the Institutional Review Board of Seoul National University Bundang Hospital and followed the tenets of the Declaration of Helsinki.

All participants underwent comprehensive ophthalmic examinations, which included assessments of the best-corrected visual acuity (BCVA), Goldmann applanation tonometry, a refraction test, slit-lamp biomicroscopy, gonioscopy, stereo disc photography, red-free fundus photography (EOS D60 digital camera; Canon, Utsunomiyashi, Japan), central corneal thickness measurement (Orbscan II; Bausch & Lomb Surgical, Rochester, NY, USA), axial length measurement (IOLMaster version 5; Carl Zeiss Meditec, Dublin, CA, USA), and corneal curvature measurement (KR-1800; Topcon, Tokyo, Japan). The peripapillary RNFL thickness was measured by spectral-domain OCT (Spectralis; Heidelberg Engineering, Heidelberg, Germany). Other ophthalmic examinations included standard automated perimetry (Humphrey Field Analyzer II 750, 24–2 Swedish interactive threshold algorithm; Carl Zeiss Meditec), enhanced depth-imaging (EDI) spectral-domain OCT scanning of the optic nerve head (ONH) (Spectralis; Heidelberg Engineering), and swept-source OCTA (DRI OCT Triton; Topcon).

The clinical history of the participants was also obtained, including demographic characteristics and the presence of cold extremities, migraine, and other systemic conditions. Systolic and diastolic blood pressures (BPs) were measured using a digital automatic BP monitor (Omron HEM-770A; Omron Matsusaka, Matsusaka, Japan). The mean arterial pressure (MAP) was calculated as diastolic BP + 1/3(systolic BP − diastolic BP), and the mean ocular perfusion pressure was calculated as 2/3(MAP − IOP) at the time of OCTA.

POAG was defined as the presence of an open iridocorneal angle, signs of glaucomatous optic nerve damage (i.e., neuroretinal rim thinning, notching, or an RNFL defect), and a glaucomatous visual field (VF) defect. A glaucomatous VF defect was defined as one conforming with one or more of the following criteria: (1) outside normal limits on a glaucoma hemifield test, (2) three abnormal points with a $<5\%$ probability of being normal and one abnormal point with a $<1\%$ probability by pattern deviation, or (3) a pattern standard deviation of probability $<5\%$ confirmed on two consecutive reliable tests (fixation loss rate of $\leq 20\%$ and false-positive error rate of $\leq 15\%$ and false-negative error rate of $\leq 25\%$).

For eyes to be included, a record was required of the untreated IOP being measured before the initiation of ocular hypotensive treatment or as identified in the referral notes. In patients with an untreated IOP ≤ 21 mm Hg, the diurnal variation was measured during office hours (every 2 hours from 9 AM to 5 PM), and the mean of the five values was considered an untreated IOP. In patients with an untreated IOP >21 mm Hg, IOP was measured twice before starting IOP-lowering medication, and the mean of the two values was considered the untreated IOP. In patients who were undergoing treatment with ocular hypotensive medication at the time of the initial visit, the diurnal variation was measured after a 4-week washout period. Eyes were also required to have been followed for at least 2.5 years, during which the RNFL thickness was measured by serial spectral-domain OCT at least five times.

The exclusion criteria were eyes with a BCVA worse than 20/40, a spherical equivalent of <-9.0 diopters (D) or $>+3.0$ D, a cylinder correction of <-3.0 D or $>+3.0$ D, a history of intraocular surgery with the exception of uneventful cataract surgery, and retinal diseases (e.g., diabetic retinopathy, retinal vessel occlusion, or retinoschisis) or neurological diseases (e.g., pituitary tumor).

Measurement of LCCI

The degree of LC deformation was assessed by measuring the LC curvature in seven locations equidistant across the vertical optic disc diameter using horizontal B-scan images obtained using EDI OCT. The corneal curvature of each eye was entered into the Spectralis OCT system before performing EDI OCT scanning to compensate for potential magnification error. The LC curvature was determined using the LC curve index (LCCI), which was defined as the degree of inflection of the curve representing a section of the LC.[26,27] The LCCI was determined by first measuring the width of anterior LC surface reference plane (*W*) and then measuring the LC curve depth (LCCD) within the anterior LC surface plane in each B-scan.

Because the extent of the visible LC differed according to the configuration of the border tissue of Elschnig, the observers evaluated the configuration of the border tissue at the temporal disc margin before measuring the LCCI, which classified it into three groups: nonoblique, internal oblique, or external oblique.[28] In the eyes with nonoblique or internal oblique border tissues, lines were drawn from each Bruch's membrane (BM) termination point perpendicular to the BM opening (BMO) reference line until they met the anterior LC surface. The line connecting the two points on the anterior LC surface was used as the reference line to measure the LCCD, which was defined as the maximum LCCD from the reference line (Fig. 1). In the eyes with externally oblique border tissue, the point where the anterior LC surface met the temporal border tissue (i.e., anterior LC insertion) was determined and the horizontal width between this point and the point below the nasal BMO was defined as *W*. The LCCD was measured from the reference line connecting the temporal anterior LC insertion point and the point on the anterior LC surface beneath the nasal BMO (Fig. 2).

The LCCI was then calculated as $(\text{LCCD}/W) \times 100$. Because the curvature was thereby normalized to the LC width, it describes the shape of the LC independent of the actual size of the ONH. Only the LC within the *W* was considered because the LC was often not clearly visible outside of this region. In eyes with LC defects, the LCCI was measured using a presumed anterior LC surface that best fit the curvature of the remaining part of the LC or excluding the area of the LC defect.

Before making the measurements, the visibility of the peripheral LC was enhanced by postprocessing the images using adaptive compensation.[29,30] Measurements were made using a manual caliper tool in the Amira software (version 5.2.2, Visage Imaging, Berlin, Germany) in seven selected B-scan images spaced equidistantly across the vertical optic disc diameter in each eye. The measurements made from the seven B-scans were used to calculate the mean LCCI of each eye.

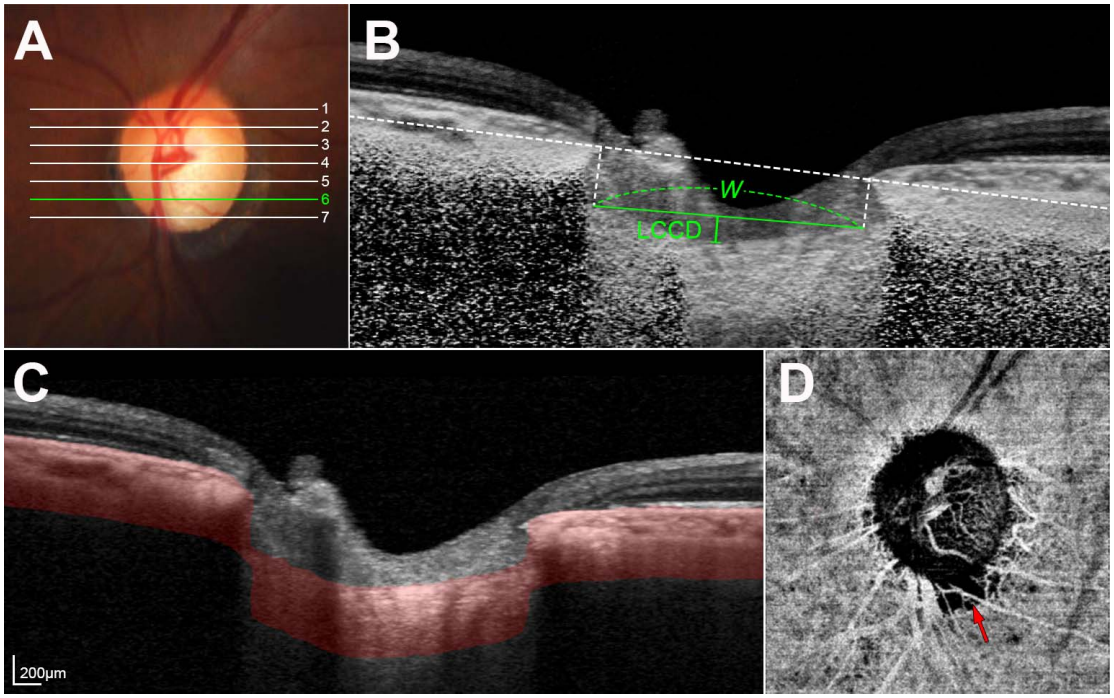

FIGURE 1. Measurement of the LCCI and determination of cMvD in an eye with internal oblique border tissue. (**A**) Color disc photograph indicating the planes where the horizontal B-scan images were obtained. (**B**) Postprocessed B-scan image obtained at plane 6 (*green line* in **A**). The LCCI was quantified by dividing the LCCD within BMO by the BMO width (*W*) and then multiplying by 100. (**C**) Horizontal B-scan image indicating the segmented layer (*red area*) to produce an en-face OCTA image (**D**). (**D**) In the en-face OCTA image, cMvD was defined as a focal sectoral capillary dropout with no visible microvascular network (*arrow*).

The LCCIs were measured by two experienced observers (JAK and EJL) who were masked to the clinical information. The average measurements made by the two observers were used in the subsequent analyses.

Assessment of Choroidal Microvasculature Dropout (cMvD) Using OCTA

The optic nerve and peripapillary area were imaged using a commercially available swept-source OCTA device (DRI OCT Triton; Topcon) with a central wavelength of 1050 nm, an acquisition speed of 100,000 A-scans per second, and axial and transverse resolutions of 7 and 20 μm in the tissue, respectively. Scans were taken from 4.5 mm × 4.5 mm cubes, with each cube consisting of 320 clusters of four repeated B-scans centered on the optic disc. En-face projections of volumetric scans allowed visualization of the structural and vascular details within segmented retinal or choroidal layers.

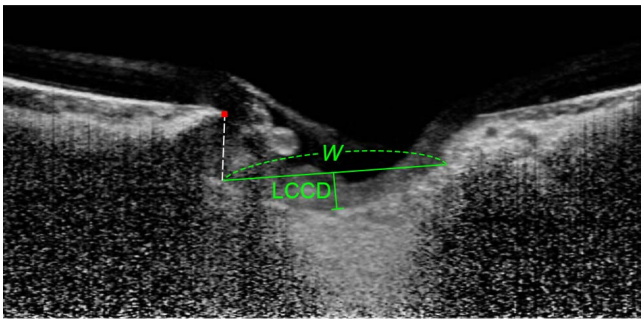

FIGURE 2. Measurement of the LCCI in an eye with externally oblique border tissue. A reference line (*horizontal green line*) was drawn between the temporal anterior LC insertion point and the point on the anterior LC surface below nasal BM termination (*red glyph*), and the width between these two points was defined as *W*. LCCD was measured from the reference line, and the LCCI was quantified by dividing the LCCD by *W* and then multiplying by 100.

The choroidal microvasculature in the peripapillary area was evaluated in en-face images of the peripapillary deep layer that were generated based on the automated layer segmentation performed by the OCT instrument software (Fig. 1). The en-face images of the deep layer were derived from an en-face slab that extended from the RPE to 390 μm below BM, which was sufficient to include the full thickness of the choroid and the inner scleral surface.

cMvD was defined as a focal sectoral capillary dropout with no visible microvascular network identified in the deep-layer en-face images.[31–33] When the circumferential width of the area with capillary dropout appeared to exceed half a clock hour of the disc circumference, it was considered as disruption of the microvascular network and so was deemed a cMvD.[32,33] Two observers (EJL and JAK) independently identified cMvDs while blinded to the clinical information of the subjects. Disagreements between these observers were resolved by a third adjudicator (T-WK). All of the included OCT B-scan images had to have image quality scores ≥30, in accordance with the manufacturer's recommendation. When the quality of the OCTA images was poor (i.e., blurred images that hampered the delineation of the cMvD), the eye was excluded from the analysis.

Data Analysis

The interobserver agreement for measuring the LCCI was evaluated by calculating the intraclass correlation coefficients (ICC). The interobserver agreement regarding confirmation of the presence of cMvD was assessed using kappa statistics (κ value). Regression analysis was used to identify the factors associated with the rate of RNFL thinning, first with a

Table 1. Demographic Characteristics of Participants

Age, y	57.1 ± 12.7 (22 to 93)
Sex, male/female	40/71
Untreated IOP, mm Hg	16.5 ± 4.1 (10.0 to 30.0)
Central corneal thickness, μm	552.4 ± 44.1 (404 to 663)
Spherical error, diopters	−1.84 ± 3.16 (−9.0 to 2.5)
Axial length, mm	24.36 ± 1.67 (21.63 to 29.10)
Global RNFL thickness, μm	71.5 ± 12.7 (48 to 103)
VF MD, dB	−5.97 ± 5.45 (−23.66 to 1.27)
DH detection, *n* (%)	53 (47.7)
β-PPA area, mm^2	0.93 ± 0.62 (0.0 to 3.5)
γ-PPA area, mm^2	0.27 ± 0.37 (0.0 to 1.8)
Diabetes mellitus, *n* (%)	16 (14.4)
Systemic hypertension, *n* (%)	32 (28.8)
Cold extremity, *n* (%)	42 (37.8)
Migraine, *n* (%)	21 (18.9)
MAP, mm Hg	91.0 ± 10.0 (68.0 to 122.0)
Mean ocular perfusion pressure, mm Hg	49.4 ± 7.9 (30.6 to 75.0)
Follow-up period, y	4.7 ± 1.0 (2.5 to 7.9)
Number of OCT examinations	7.0 ± 1.5 (5 to 11)
LCCI	9.11 ± 3.26 (1.76 to 18.42)
Presence of cMvD, *n* (%)	75 (67.6)
Rate of RNFL thinning, μm/y	−1.52 ± 0.96 (−4.30 to 0.77)

MD, mean deviation.

univariate model and then with a multivariate model that included variables from the univariate model for which $P < 0.10$.

The regression tree model was additionally used to stratify patients with faster or slower OCT RNFL thinning, based on the factors influencing this rate of RNFL thinning.[25] All possible splits of this type were considered, with the one that best separated the data into groups being chosen. The end points of this tree were the rate of OCT RNFL thinning (microns per year). Factors that were found to be associated with the rate of OCT RNFL thinning in the univariate regression analysis were implanted as possible risk factors. A 10-fold cross validation was performed to remove any insignificant splits. In addition, simulation experiments were carried out 10,000 times using the bootstrap technique. This analysis was performed using the rpart package in R (version 2.2.1; available at http://www.rproject.org, accessed May 27, 2018).

Subgroups classified from the regression tree analysis were compared using analysis of variance with the Bonferroni post hoc test. Statistical analyses other than regression tree analysis were performed using the Statistical Package for the Social Sciences (version 22.0; SPSS, Chicago, IL, USA). Probability values of $P < 0.05$ were considered indicative of statistical significance. Except where stated otherwise, the data are presented as mean ± SD values.

Results

A total of 120 POAG eyes that underwent an OCTA examination and had serial OCT RNFL thickness measurements made during >2.5 years were initially included. Nine of these eyes were excluded because of poor-quality OCTA images; the baseline characteristics of the remaining 111 POAG eyes are provided in Table 1. There was excellent interobserver agreement regarding the measured LCCI values (ICC = 0.988, 95% confidence interval = 0.983–0.992) and the detection of cMvD (κ = 0.958).

Identification of Factors Associated With the Rate of Global RNFL Thinning

Factors associated with the rate of global RNFL thinning were identified using a general linear model. Univariate analysis revealed that a larger global RNFL thickness, a higher VF mean deviation, a larger β-PPA area, a larger LCCI, and the presence of cMvD were associated significantly with faster RNFL thinning. In multivariate analysis, the rate of global RNFL thinning was influenced significantly by DH during follow-up, larger LCCI, and presence of cMvD (Table 2).

Table 2. Factors Associated With the Rate of RNFL Change

	Univariate Analysis			Multivariate Analysis		
	Beta	**95% CI**	***P***	**Beta**	**95% CI**	***P***
Age, per 1 year older	−0.002	−0.016 to 0.012	0.778			
Sex, female	0.153	−0.224 to 0.531	0.422			
Untreated IOP, per 1 mm Hg higher	−0.042	−0.086 to 0.003	0.065	−0.033	−0.072 to 0.005	0.091
Central corneal thickness, per 1 μm thicker	−0.003	−0.007 to 0.002	0.209			
Axial length, per 1 mm longer	−0.042	−0.165 to 0.080	0.494			
Global RNFL thickness, per 1 μm thicker	−0.016	−0.030 to −0.002	**0.028**	−0.008	−0.022 to 0.007	0.308
VF MD, per dB higher	−0.036	−0.069 to −0.003	0.031	−0.032	−0.065 to 0.001	0.061
DH detection	−0.354	−0.712 to 0.003	0.052	−0.150	−0.528 to 0.229	**0.013**
β-PPA area, per 1 mm^2 larger	−0.293	−0.581 to −0.005	**0.046**	−0.221	−0.480 to 0.035	0.094
γ-PPA area, per 1 mm^2 larger	0.289	−0.200 to 0.779	0.244			
Diabetes mellitus	−0.040	−0.556 to 0.477	0.879			
Systemic hypertension	0.174	−0.227 to 0.575	0.391			
Cold extremity	−0.131	−0.515 to 0.252	0.498			
Migraine	−0.341	−0.807 to 0.125	0.150			
MAP, per 1 mm Hg higher	−0.008	−0.026 to 0.010	0.378			
Mean ocular perfusion pressure, per 1 mm Hg higher	0.010	−0.013 to 0.033	0.387			
Follow-up period, per 1 year longer	−0.001	−0.181 to 0.179	0.987			
Number of OCT examination	−0.099	−0.222 to 0.024	0.113			
LCCI, per 1 unit larger	−0.106	0.054 to 0.158	**<0.001**	−0.097	−0.146 to −0.048	**<0.001**
Presence of cMvD	−0.453	−0.832 to −0.075	**0.019**	−0.389	−0.850 to 0.072	**<0.001**

Statistically significant values are shown in bold. CI, confidence interval.

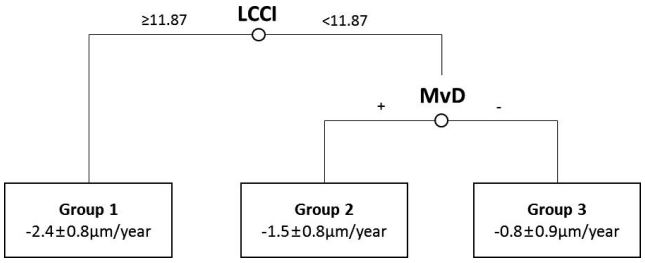

FIGURE 3. The regression tree model stratifying the groups with faster or slower progression based on the factors best explaining the rate of RNFL thinning.

Regression Tree

The regression tree model, which considered seven factors identified in the univariate regression analysis as possible risk factors, revealed the two strongest discriminating variables, which produced three groups with different rate of RNFL thinning (Fig. 3). The strongest discriminating variable was LCCI. Eyes with an LCCI ≥11.87 exhibited the fastest RNFL thinning (group 1; −2.4 ± 0.8 μm/year, $n = 22$; Fig. 4), and no further splitting was necessary in that arm. When the LCCI was <11.87, the next-strongest discriminating variable was the presence or absence of cMvD. The presence of cMvD was associated with faster RNFL thinning (group 2; −1.5 ± 0.8 μm/year, $n = 63$; Fig. 5), whereas the absence of cMvD was associated with slower RNFL thinning (group 3; −0.8 ± 0.9 μm/year, $n = 26$; Fig. 6). Of the 10,000 times simulation experiments, LCCI was detected as the strongest discriminating variable 8291 times and the cMvD was detected as the strongest discriminating variable in patients with the LCCI <11.87. The mean split of LCCI at the root node from 10,000 simulations was 11.86. The simulation standard deviation of the split was 1.19.

Comparison among the three groups classified from the regression tree revealed that the untreated IOP was higher, the β-PPA area was larger, and the follow-up period was shorter in group 1 than in group 3 (Table 3). Eyes in group 2 were more myopic and had a thinner baseline RNFL and a larger β-PPA area than the eyes in group 3 (Table 3).

DISCUSSION

The study created a regression tree to explain the future rate of progressive RNFL thinning in POAG. A larger LCCI was the most important prognostic factor for faster RNFL thinning, followed by the presence of cMvD, which was the strongest influencing factor in the eyes with a smaller LCCI. Eyes having a smaller LCCI and no cMvD had the slowest RNFL thinning.

Currently available OCT devices can image the LC in the horizontal, vertical, and radial directions. In the present study, LC-related parameters were measured on horizontal B-scan images. Because the LC possesses a bowtie-shaped central ridge,[34] LC shape typically appears as a W-shape in vertical scans, and varies largely in radial scans along the meridians (Fig. 7A). Accordingly, it is difficult to assess the LC shape using a simple parameter such as LCCI in vertical or radial scans. In contrast, the LC has a relatively regular configuration in the horizontal plane, with a flat or U-shaped appearance with different regional steepness (Fig. 7B). Therefore, the LC shape can be readily evaluated on horizontal scans using LCCI.[35–37] Moreover, measuring LCCI on horizontal scans allows separate assessment of the LC morphologies in the superior and inferior region, which are often different in an individual eye.[36]

Considering the importance of posterior deformation of the LC in glaucoma, it is not surprising that the LCCI was the most important prognostic factor for progressive RNFL thinning. This finding is consistent with previous demonstrations of glaucoma progression being influenced by the LC deformation assessed by measuring the level of the anterior LC surface from BM (i.e., LC depth). However, recent studies have demonstrated that the LC curvature (i.e., LCCI) is superior to the LC depth as an indicator of mechanical strain.[27,38] In addition, the LCCI was a better prognostic factor of both the development[11] and progression[39] of glaucoma than was the LC depth.

TABLE 3. Comparison Between Groups Divided by Regression Tree Analysis

	Group 1, $n = 22$	Group 2, $n = 63$	Group 3, $n = 26$	*P*	Post hoc
Rate of RNFL thinning, μm/y	−2.4 ± 0.8	−1.5 ± 0.8	−0.8 ± 0.9	**<0.001**	1<2<3
LCCI	13.7 ± 1.7	7.6 ± 2.5	8.8 ± 2.2	**<0.001**	1>3>2
Presence of cMvD, *n* (%)	12 (54.5)	63 (100)	0 (0)	**<0.001**	
Age, y	59.4 ± 13.3	55.3 ± 11.6	59.5 ± 14.2	0.235	
Sex, male/female	10/12	24/39	6/20	0.240	
Untreated IOP, mm Hg	17.9 ± 4.9	16.7 ± 4.2	15.1 ± 2.5	0.057	1>3
Central corneal thickness, μm	556.1 ± 42.7	550.7 ± 48.1	553.2 ± 36.3	0.886	
Spherical error, D	−1.4 ± 3.2	−2.4 ± 3.1	−0.9 ± 3.1	0.101	2<3
Axial length, mm	24.39 ± 1.59	24.62 ± 1.73	23.65 ± 1.38	0.072	2>3
Global RNFL thickness, μm	74.6 ± 12.9	68.6 ± 11.7	75.9 ± 13.5	**0.021**	2<3
VF MD, dB	−4.95 ± 4.59	−6.76 ± 5.48	−4.92 ± 5.91	0.218	
DH detection, *n* (%)	10 (45.4)	25 (39.7)	12 (46.2)	0.809	
β-PPA area, mm^2	1.17 ± 0.64	0.98 ± 0.61	0.62 ± 0.52	**0.005**	1=2>3
γ-PPA area, mm^2	0.19 ± 0.38	0.33 ± 0.35	0.17 ± 0.40	0.087	
Diabetes mellitus, *n* (%)	2 (9.1)	11 (17.5)	3 (11.5)	0.501	
Systemic hypertension, *n* (%)	4 (18.2)	16 (25.4)	12 46.2)	0.080	
Cold extremity, *n* (%)	9 (40.9)	20 (31.7)	13 (50.0)	0.324	
Migraine, *n* (%)	3 (13.6)	14 (22.2)	3 (11.5)	0.302	
MAP, mm Hg	94.4 ± 9.0	89.5 ± 9.0	91.8 ± 12.4	0.161	
Mean ocular perfusion pressure, mm Hg	50.8 ± 5.9	48.4 ± 8.3	50.3 ± 8.3	0.403	
Follow-up period, y	4.4 ± 1.2	4.6 ± 0.9	5.0 ± 1.2	0.108	1<3
Number of OCT examination	7.1 ± 1.2	7.0 ± 1.7	7.0 ± 1.2	0.882	

Statistically significant values are shown in bold.

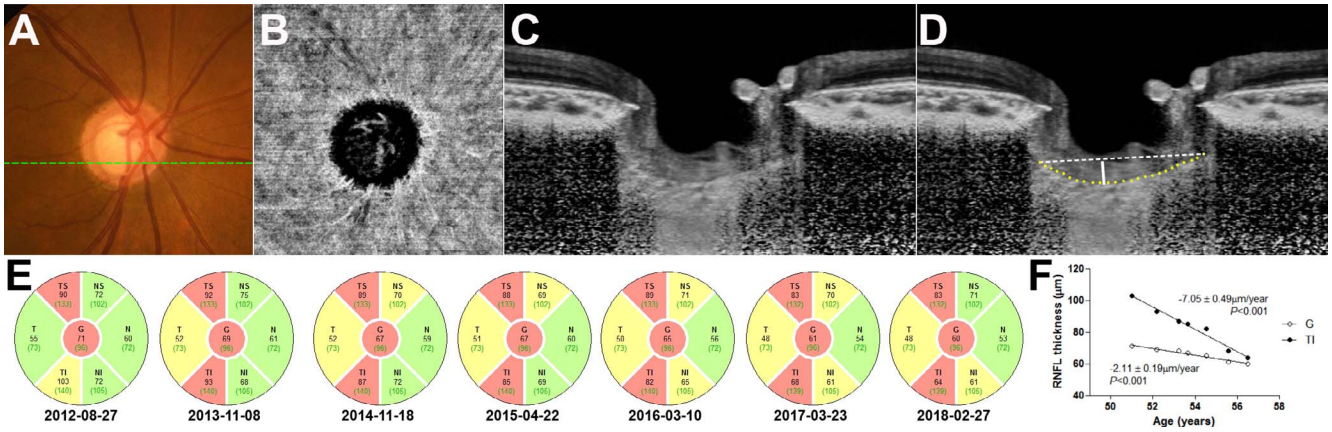

Figure 4. A glaucomatous eye in the fastest-progression group (group 1) with a larger LCCI and not having a cMvD. (**A**) Color disc photograph. (**B**) En-face OCTA image of the choroidal layer. (**C**) Postprocessed B-scan image obtained at the inferotemporal optic nerve (indicated by *dashed line* in **A**). (**D**) Same image as (**C**) with labeling. *Yellow dotted line*, anterior LC surface; *white dashed line*, reference line; *solid line*, LCCD. The LCCI was 15.0 in this eye. (**E**) OCT circular diagrams showing serial changes in the RNFL thickness in six sectors: temporal-superior (TS), temporal (T), temporal-inferior (TI), nasal-inferior (NI), nasal (N), and nasal-superior (NS). (**F**) Linear regression lines showing rates of global RNFL thinning and sectoral RNFL thinning in the TI sector.

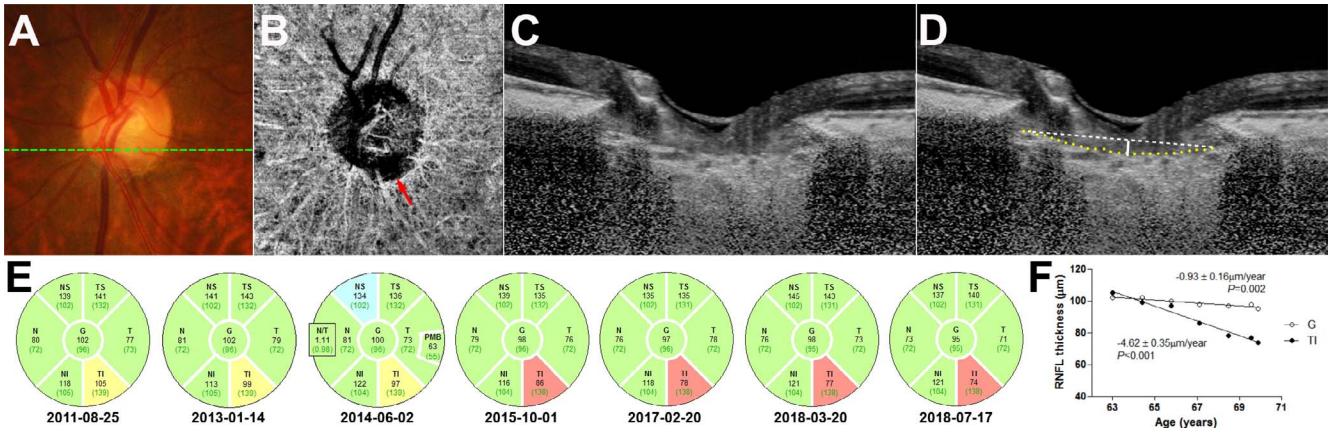

Figure 5. A glaucomatous eye in the group with the second fastest progression (group 2) with a smaller LCCI and having a cMvD. (**A**) Color disc photograph. (**B**) En-face OCTA image of the choroidal layer. *Arrow* indicates a cMvD. (**C**) Postprocessed B-scan image obtained at the inferotemporal optic nerve (indicated by *dashed line* in **A**). (**D**) Same image as (**C**) with labeling. *yellow dotted line*, anterior LC surface; *white dashed line*, reference line; *solid line*, LCCD. The LCCI was 8.8 in this eye. (**E**) OCT circular diagrams showing serial changes in the RNFL thickness in six sectors: TS, T, TI, NI, N, and NS. (**F**) Linear regression lines showing rates of global RNFL thinning and sectoral RNFL thinning in the TI sector.

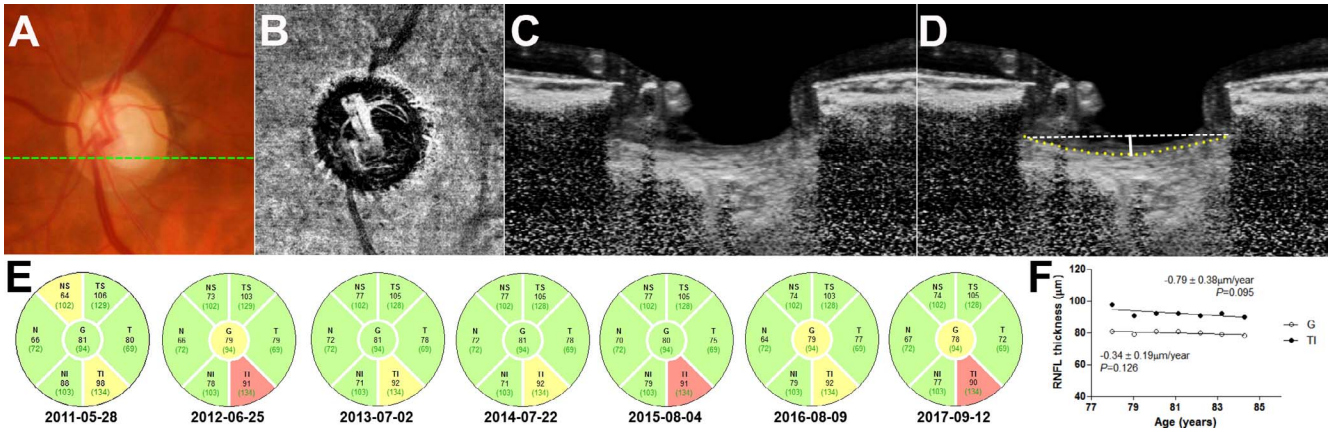

Figure 6. A glaucomatous eye in the group with the slowest progression (group 3) with a smaller LCCI and not having a cMvD. (**A**) Color disc photograph. (**B**) En-face OCTA image of the choroidal layer. (**C**) Postprocessed B-scan image obtained at the inferotemporal optic nerve (indicated by *dashed line* in **A**). (**D**) Same image as (**C**) with labeling. *Yellow dotted line*, anterior LC surface; *white dashed line*, reference line; *solid line*, LCCD. The LCCI was 8.8 in this eye. (**E**) OCT circular diagrams showing serial changes in the RNFL thickness in six sectors: TS, T, TI, NI, N, and NS. (**F**) Linear regression lines showing rates of global RNFL thinning and sectoral RNFL thinning in the TI sector.

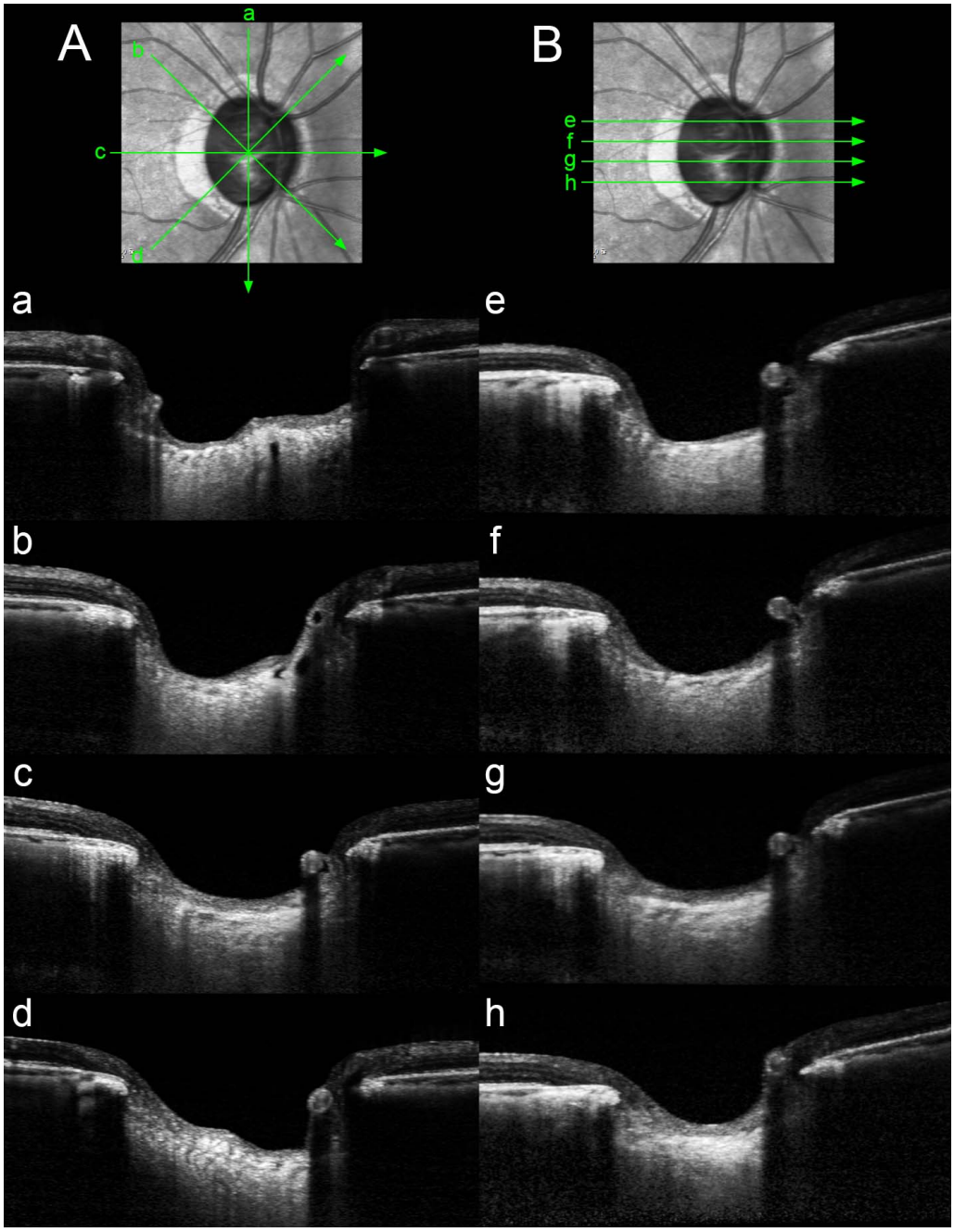

FIGURE 7. Comparison of the patterns of the LC shape in radial (**A**), and horizontal (**B**) B-scans. Note that the largely different pattern of LC shape in radial scans because of the bowtie-shaped central ridge (**A**). In contrast, the LC has a relatively regular configuration in the horizontal scans, with a flat or U-shaped appearance with different regional steepness (**B**).

The presence of cMvD was revealed as another important factor for faster RNFL thinning, particularly in eyes with a smaller LCCI. This is consistent with a recent study showing the association of cMvD with progressive RNFL thinning in POAG.[24] A cMvD corresponds to the perfusion defect as assessed by indocyanine-green angiography, indicating that cMvD represents a true vascular compromise.[33] Although the pathogenic importance of cMvD remains to be determined, assuming that it occurs as a primary event, the existence of cMvD suggests vascular insufficiency in the prelaminar or laminar tissue because the short posterior ciliary artery supplies both the parapapillary choroid and the deep ONH tissue. Axonal transport is an energetically costly process that is performed by adenosine-5′-triphosphate-dependent motor proteins such as dynein.[40] Therefore, hypoperfusion in the deep ONH tissue will hamper the axonal transport of neurotrophic factors to the cell body, which in turn promotes the apoptosis of retinal ganglion cells.[41] On the other hand, it is also possible that cMvD is secondary to glaucomatous optic nerve damage (i.e., reduced metabolic need because of the damaged optic nerve). However, even in this situation, cMvD may still play a role in the progression of glaucomatous optic nerve damage. The ischemia in the area of cMvD may disrupt the blood–optic-nerve barrier, which in turn would allow the release of vasoactive or toxic substances into the ONH that may damage the remaining optic nerve axons. The strong

Table 4. Relationship Between the Presence of cMvD and PPA

	Eyes With cMvD, $n = 75$	Eyes Without cMvD, $n = 36$	P
Presence of β-PPA, n (%)	73 (97.3)	31 (86.1)	0.023*
Presence of γ-PPA, n (%)	44 (58.7)	8 (22.2)	<0.001*
β-PPA area, mm^2	1.04 ± 0.64	0.72 ± 0.53	0.012†
γ-PPA area, mm^2	0.33 ± 0.37	0.13 ± 0.34	0.006†

* Pearson's χ^2 test
† *t*-test for independent samples.

influence of cMvD on the rate of RNFL thinning in eyes with smaller LCCI suggests that vascular factors are particularly important in glaucoma progression when the LC is not greatly deformed.

The groups determined when formulating the regression tree model exhibited different clinical characteristics apart from LCCI and the presence of cMvD. The most distinctive feature in the fastest-progression group (group 1) was a higher untreated IOP, which might have been due to the deformed LC associated with increased IOP imposing a sustained stress on the ONH axons resulting in ongoing progressive RNFL thinning. On the other hand, eyes in the group with the second fastest progression (group 2) with a smaller LCCI but having cMvD tended to be more myopic and have a longer axial length than did those in the group with the slowest progression (group 3). This finding is consistent with previous reports of an association between cMvD and myopia.[24,42] It has also been suggested that scleral vessels can be subjected to tensile stress associated with axial elongation of globe that causes cMvD of the choroidal layer.[42]

Although DH was a significant factor associated with rapid RNFL thinning in the conventional regression analysis, it was not presented as a prognostic factor in the regression tree model. DH is a known strong risk factor for glaucoma progression[13,43,44] and may indicate ongoing glaucomatous damage.[45–47] It is possible that that some DH was left undetected between the follow-ups by paucity of optic disc examinations, which have weakened the influence of DH on the rate of RNFL thinning.

The univariate analysis in the present study indicated that the β-PPA area significantly influenced the rate of RNFL thinning, which is consistent with previous findings.[10,19] However, this association was only marginally significant in the multivariate analysis. The disappearance of the β-PPA area in the multivariate analysis appears to be due to the association between β-PPA and cMvD, with cMvD found exclusively within the β- or γ-PPA region in both the present (Table 4) and previous studies.[24,31,48,49] This finding further suggests that cMvD has a stronger influence on the rate of RNFL thinning than β-PPA does. Although the precise relationship between cMvD and β-PPA remains to be clarified, the significant influence of β-PPA on glaucoma progression may be due to the higher likelihood of the presence of cMvD in those eyes.

Our study has limitations. First, the cMvD was documented during the follow-up rather than at the beginning of the study. Therefore, causal relationship between cMvD and progressive RNFL thinning could not be clarified. A future prospective study is required to reveal the pathogenic significance of a cMvD in glaucomatous optic neuropathy. Second, regression tree analysis may provide less accurate results compared with linear regression analysis when continuous variables are used. It may also overfit data. However, we performed simulation experiments 10,000 times, which showed the same tree structure in most of the experiments and similar cutoff value for LCCI. Therefore, we consider that the tree structure is not overfitted and the cutoff of the LCCI may be deemed stable.

In conclusion, this study has developed a systematic prognostic model for the rate of progressive RNFL thinning in POAG, in which a larger LCCI and the presence of cMvD are strongest factors for faster RNFL thinning. The findings of the present study may allow stratification of the risk of faster progression in POAG patients and represent valuable information for making treatment decisions.

Acknowledgments

Supported by the Seoul National University Bundang Hospital Research Fund (no. 02-2016-023), and by Basic Science Research program through the National Research Foundation of Korea funded by the Ministry of Education, Science, and Technology, Seoul, South Korea (no. 2016R1D1A1B02011696). The funder had no role in the design or conduct of this research.

Disclosure: **E.J. Lee**, None; **T.-W. Kim**, None; **J.-A. Kim**, None; **G.-N. Kim**, None; **J.M. Kim**, None; **M.J.A. Girard**, None; **J.M. Mari**, None; **H. Kim**, None

References

1. Quigley HA, Addicks EM, Green WR, Maumenee AE. Optic nerve damage in human glaucoma. II. The site of injury and susceptibility to damage. *Arch Ophthalmol*. 1981;99:635–649.
2. Bellezza AJ, Rintalan CJ, Thompson HW, Downs JC, Hart RT, Burgoyne CF. Deformation of the lamina cribrosa and anterior scleral canal wall in early experimental glaucoma. *Invest Ophthalmol Vis Sci*. 2003;44:623–637.
3. Yang H, Downs JC, Bellezza A, Thompson H, Burgoyne CF. 3-D histomorphometry of the normal and early glaucomatous monkey optic nerve head: prelaminar neural tissues and cupping. *Invest Ophthalmol Vis Sci*. 2007;48:5068–5084.
4. Strouthidis NG, Fortune B, Yang H, Sigal IA, Burgoyne CF. Longitudinal change detected by spectral domain optical coherence tomography in the optic nerve head and peripapillary retina in experimental glaucoma. *Invest Ophthalmol Vis Sci*. 2011;52:1206–1219.
5. Burgoyne CF, Downs JC, Bellezza AJ, Suh JK, Hart RT. The optic nerve head as a biomechanical structure: a new paradigm for understanding the role of IOP-related stress and strain in the pathophysiology of glaucomatous optic nerve head damage. *Prog Retin Eye Res*. 2005;24:39–73.
6. Anderson DR, Hendrickson A. Effect of intraocular pressure on rapid axoplasmic transport in monkey optic nerve. *Invest Ophthalmol*. 1974;13:771–783.
7. Minckler DS, Bunt AH, Johanson GW. Orthograde and retrograde axoplasmic transport during acute ocular hypertension in the monkey. *Invest Ophthalmol Vis Sci*. 1977;16:426–441.
8. Minckler DS, Tso MO. A light microscopic, autoradiographic study of axoplasmic transport in the normal rhesus optic nerve head. *Am J Ophthalmol*. 1976;82:1–15.
9. Hernandez MR. The optic nerve head in glaucoma: role of astrocytes in tissue remodeling. *Prog Retin Eye Res*. 2000;19:297–321.
10. Lee EJ, Kim TW, Kim M, Kim H. Influence of lamina cribrosa thickness and depth on the rate of progressive retinal nerve fiber layer thinning. *Ophthalmology*. 2015;122:721–729.
11. Kim JA, Kim TW, Weinreb RN, Lee EJ, Girard MJA, Mari JM. Lamina cribrosa morphology predicts progressive retinal nerve fiber layer loss in eyes with suspected glaucoma. *Sci Rep*. 2018;8:738.
12. Weinreb RN, Khaw PT. Primary open-angle glaucoma. *Lancet*. 2004;363:1711–1720.

13. Leske MC, Heijl A, Hyman L, et al. Predictors of long-term progression in the early manifest glaucoma trial. *Ophthalmology*. 2007;114:1965–1972.
14. Kaiser HJ, Flammer J, Graf T, Stumpfig D. Systemic blood pressure in glaucoma patients. *Graefes Arch Clin Exp Ophthalmol*. 1993;231:677–680.
15. Flammer J, Orgul S, Costa VP, et al. The impact of ocular blood flow in glaucoma. *Prog Retin Eye Res*. 2002;21:359–393.
16. Gherghel D, Orgul S, Gugleta K, Gekkieva M, Flammer J. Relationship between ocular perfusion pressure and retrobulbar blood flow in patients with glaucoma with progressive damage. *Am J Ophthalmol*. 2000;130:597–605.
17. Lee EJ, Kim TW, Weinreb RN, Park KH, Kim SH, Kim DM. beta-Zone parapapillary atrophy and the rate of retinal nerve fiber layer thinning in glaucoma. *Invest Ophthalmol Vis Sci*. 2011; 52:4422–4427.
18. Teng CC, De Moraes CG, Prata TS, Tello C, Ritch R, Liebmann JM. Beta-Zone parapapillary atrophy and the velocity of glaucoma progression. *Ophthalmology*. 2010;117:909–915.
19. Kim YW, Lee EJ, Kim TW, Kim M, Kim H. Microstructure of beta-zone parapapillary atrophy and rate of retinal nerve fiber layer thinning in primary open-angle glaucoma. *Ophthalmology*. 2014;121:1341–1349.
20. Yamada H, Akagi T, Nakanishi H, et al. Microstructure of peripapillary atrophy and subsequent visual field progression in treated primary open-angle glaucoma. *Ophthalmology*. 2016;123:542–551.
21. Leske MC, Heijl A, Hussein M, et al. Factors for glaucoma progression and the effect of treatment: the early manifest glaucoma trial. *Arch Ophthalmol*. 2003;121:48–56.
22. Kim SH, Park KH. The relationship between recurrent optic disc hemorrhage and glaucoma progression. *Ophthalmology*. 2006;113:598–602.
23. Kim KE, Jeoung JW, Kim DM, Ahn SJ, Park KH, Kim SH. Long-term follow-up in preperimetric open-angle glaucoma: progression rates and associated factors. *Am J Ophthalmol*. 2015;159:160–168.
24. Park HL, Kim JW, Park CK. Choroidal microvasculature dropout is associated with progressive retinal nerve fiber layer thinning in glaucoma with disc hemorrhage. *Ophthalmology*. 2018;125:1003–1013.
25. Therneau T, Atkinson B, Ripley B, Ripley MB. Package 'rpart'. Available at: https://cran.r-project.org/web/packages/rpart/rpart.pdf. Accessed April 20, 2016.
26. Lee SH, Yu DA, Kim TW, Lee EJ, Girard MJ, Mari JM. Reduction of the lamina cribrosa curvature after trabeculectomy in glaucoma. *Invest Ophthalmol Vis Sci*. 2016;57:5006–5014.
27. Lee SH, Kim TW, Lee EJ, Girard MJ, Mari JM. Diagnostic power of lamina cribrosa depth and curvature in glaucoma. *Invest Ophthalmol Vis Sci*. 2017;58:755–762.
28. Reis AS, Sharpe GP, Yang H, Nicolela MT, Burgoyne CF, Chauhan BC. Optic disc margin anatomy in patients with glaucoma and normal controls with spectral domain optical coherence tomography. *Ophthalmology*. 2012;119:738–747.
29. Girard MJ, Strouthidis NG, Ethier CR, Mari JM. Shadow removal and contrast enhancement in optical coherence tomography images of the human optic nerve head. *Invest Ophthalmol Vis Sci*. 2011;52:7738–7748.
30. Mari JM, Strouthidis NG, Park SC, Girard MJ. Enhancement of lamina cribrosa visibility in optical coherence tomography images using adaptive compensation. *Invest Ophthalmol Vis Sci*. 2013;54:2238–2247.
31. Suh MH, Zangwill LM, Manalastas PI, et al. Deep retinal layer microvasculature dropout detected by the optical coherence tomography angiography in glaucoma. *Ophthalmology*. 2016; 123:2509–2518.
32. Lee EJ, Kim TW, Lee SH, Kim JA. Underlying microstructure of parapapillary deep-layer capillary dropout identified by optical coherence tomography angiography. *Invest Ophthalmol Vis Sci*. 2017;58:1621–1627.
33. Lee EJ, Lee KM, Lee SH, Kim TW. Parapapillary choroidal microvasculature dropout in glaucoma: a comparison between optical coherence tomography angiography and indocyanine green angiography. *Ophthalmology*. 2017;124: 1209–1217.
34. Park SC, Kiumehr S, Teng CC, Tello C, Liebmann JM, Ritch R. Horizontal central ridge of the lamina cribrosa and regional differences in laminar insertion in healthy subjects. *Invest Ophthalmol Vis Sci*. 2012;53:1610–1616.
35. Lee EJ, Kim TW, Kim H, Lee SH, Girard MJ, Mari JM. Comparison between lamina cribrosa depth and curvature as a predictor of progressive retinal nerve fiber layer thinning in primary open-angle glaucoma. *Ophthalmol Glaucoma*. 2018;1:44–51.
36. Kim JA, Kim TW, Lee EJ, Girard MJA, Mari JM. Lamina cribrosa morphology in glaucomatous eyes with hemifield defect in a Korean population. *Ophthalmology*. 2019;126:692–701.
37. Lee SH, Kim TW, Lee EJ, Girard MJA, Mari JM. Lamina cribrosa curvature in healthy Korean eyes. *Sci Rep*. 2019;9:1756.
38. Vianna JR, Lanoe VR, Quach J, et al. Serial changes in lamina cribrosa depth and neuroretinal parameters in glaucoma: impact of choroidal thickness. *Ophthalmology*. 2017;124: 1392–1402.
39. Ha A, Kim TJ, Girard MJA, et al. Baseline lamina cribrosa curvature and subsequent visual field progression rate in primary open-angle glaucoma. *Ophthalmology*. 2018;125: 1898–1906.
40. Maday S, Twelvetrees AE, Moughamian AJ, Holzbaur EL. Axonal transport: cargo-specific mechanisms of motility and regulation. *Neuron*. 2014;84:292–309.
41. Osborne NN. Mitochondria: their role in ganglion cell death and survival in primary open angle glaucoma. *Exp Eye Res*. 2010;90:750–757.
42. Lee EJ, Kim TW, Kim JA, Kim JA. Parapapillary deep-layer microvasculature dropout in primary open-angle glaucoma eyes with a parapapillary gamma-zone. *Invest Ophthalmol Vis Sci*. 2017;58:5673–5680.
43. Chan TCW, Bala C, Siu A, Wan F, White A. Risk factors for rapid glaucoma disease progression. *Am J Ophthalmol*. 2017; 180:151–157.
44. Akagi T, Zangwill LM, Saunders LJ, et al. Rates of local retinal nerve fiber layer thinning before and after disc hemorrhage in glaucoma. *Ophthalmology*. 2017;124:1403–1411.
45. Nitta K, Sugiyama K, Higashide T, Ohkubo S, Tanahashi T, Kitazawa Y. Does the enlargement of retinal nerve fiber layer defects relate to disc hemorrhage or progressive visual field loss in normal-tension glaucoma? *J Glaucoma*. 2011;20:189–195.
46. Lee EJ, Kim TW, Kim M, Girard MJ, Mari JM, Weinreb RN. Recent structural alteration of the peripheral lamina cribrosa near the location of disc hemorrhage in glaucoma. *Invest Ophthalmol Vis Sci*. 2014;55:2805–2815.
47. Lee EJ, Han JC, Kee C. A novel hypothesis for the pathogenesis of glaucomatous disc hemorrhage. *Prog Retin Eye Res*. 2017;60:20–43.
48. Lee EJ, Kim TW, Kim JA, Kim JA. Central visual field damage and parapapillary choroidal microvasculature dropout in primary open-angle glaucoma. *Ophthalmology*. 2018;125: 588–596.
49. Akagi T, Iida Y, Nakanishi H, et al. Microvascular density in glaucomatous eyes with Hemifield visual field defects: an optical coherence tomography angiography study. *Am J Ophthalmol*. 2016;168:237–249.

Investigative Ophthalmology & Visual Science